Journal of Molecular Structure 1211 (2020) 128105

Contents lists available at ScienceDirect

Journal of Molecular Structure

journal homepage: http://www.elsevier.com/locate/molstruc

Photo-dynamic and fluorescent zinc complex based on spiropyran ligand

Flávio B. Miguez [a], Thiago G. Menzonatto [b], Jorge Fernandes Z. Netto [a], Igor M.S. Silva [c], Thiago Verano-Braga [c], Juliana Fedoce Lopes [b], Frederico B. De Sousa [a, *]

[a] Laboratório de Sistemas Poliméricos e Supramoleculares (LSPS) – Instituto de Física e Química, Universidade Federal de Itajubá (UNIFEI), Itajubá, 37500-903, MG, Brazil
[b] Laboratório de Química Computacional (LaQC) – Instituto de Física e Química, Universidade Federal de Itajubá (UNIFEI), Itajubá, 37500-903, MG, Brazil
[c] Departamento de Fisiologia e Biofísica - Instituto de Ciências Biológicas, Universidade Federal de Minas Gerais (UFMG), Belo Horizonte, 31270-901, MG, Brazil

ARTICLE INFO

Article history:
Received 15 January 2020
Received in revised form
16 March 2020
Accepted 19 March 2020
Available online 20 March 2020

Keywords:
Zinc
Spiropyran
Coordination complex
Chromism
Computational calculations

ABSTRACT

Spiropyrans are among a class of organic molecules widely studied as molecular photoswitches. A photochromic and solvatochromic spiropyran-containing Zinc (II) complex (ZnMC) was successfully synthesized and characterized, and its chromic properties were studied. A solid complex was isolated through a precipitation process induced by UV radiation. The binding specificities were studied by FTIR-ATR spectroscopy and DFT calculations, demonstrating that phenolate and carboxylic acid are the binding sites of merocyanine. Mass spectrometry and computational methods revealed the possibility of two complexes with different geometries, tetrahedral and octahedral; the complex with tetrahedral characteristics proved to be more stable and abundant. ZnMC solvatochromic properties were analyzed, presenting a wide variation in its absorption band in the visible region. We addressed the issue of ZnMC photodegradation in different solvents, and the observed absorbance did not vary after the first cycles for acetonitrile, while, in tetrahydrofuran, the absorbance decayed throughout the 48 cycles of switching between UV and visible light irradiation.

1. Introduction

Metal ions are known to exhibit an exceedingly wide variety of applications in chemical and biomedical processes [1–3]. There is also a great interest in the area of identifying these metal ions, with a growing interest in the development of new molecules that can be used as sensors for specific metals [4]. In regard to zinc, this metal has been used in interesting biological applications, such as in building blocks for porous anionic bio-MOFs, used to store and release drug molecules through a cation-triggered system [5]. Barman and co-workers showed that zinc complexes can be used in processes of catalysis, reporting a new zinc complex containing bulky guanidinate and amino ligands, used as a catalyst for the intramolecular hydroamination reaction of primary and secondary amino olefins [6]. Murugan described for the first time the synthesis of a zinc complex attached in a quinoline heterocyclic ring, used as a detector of AsO^{2-} and H_2PO^{4-} ions in aqueous dimethylsulfoxide [7].

More recently, many molecules have been used as ligands of coordination complexes; the composition of these ligands can be modulated according to the desirable properties, and the response to an external stimulus that induces chromism is an interesting one [8]. Molecules that have chromic properties are gaining certain importance in the scientific area; in this context, it is worth highlighting the spiropyrans, a class of photochromic organic molecules containing two interconnected cycles through a single atom, usually a quaternary carbon [9,10].

Spiropyrans are usually stable in a colorless closed ring form, called the spiro form (SP), and, when exposed to ultraviolet radiation, suffer a reversible isomerization process creating the merocyanine form (MC), which has an open ring and presents color varying with the chemical environment (Fig. 1) [11,12]. This process

* Corresponding author. Laboratório de Sistemas Poliméricos e Supramoleculares (LSPS) – Instituto de Física e Química, Universidade Federal de Itajubá (UNIFEI), Itajubá, 37500-903, MG, Brazil.,
E-mail address: fredbsousa@unifei.edu.br (F.B. De Sousa).

https://doi.org/10.1016/j.molstruc.2020.128105
0022-2860/

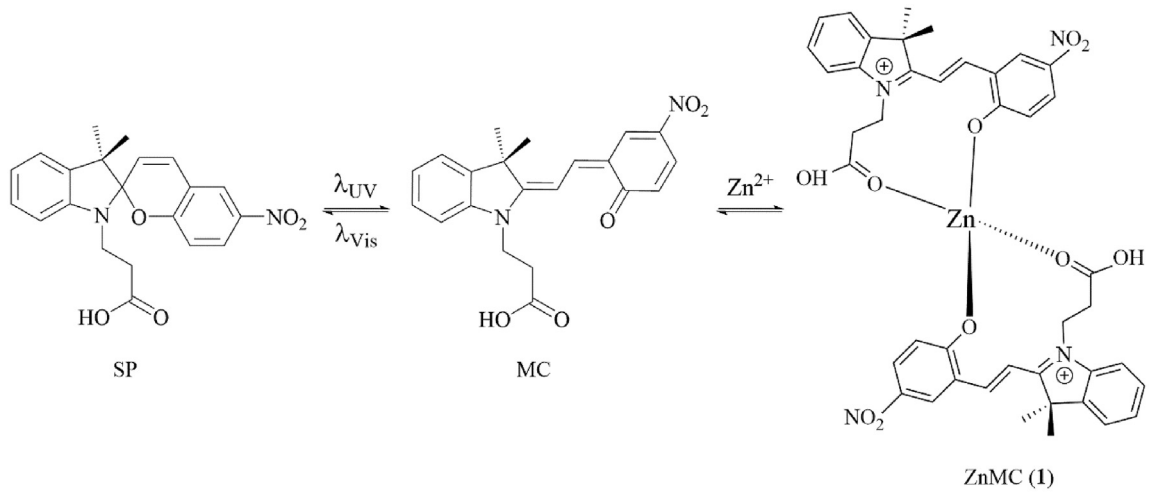

Fig. 1. Schematic representation of SPCOOH's isomers and the coordination reaction between MC and Zn^{2+}.

occurs through a heterolytic C—O bond breaking, followed by a rotation of the molecule, leading to an increase of the system's conjugation based on the formation of new π bonds [13,14]. This class of molecules has unique and distinct properties between their two isomers; among them, the following are the most prominent: the increase of the dipole moment due to the charge separation present in MC form, which can be confirmed with Time-Dependent Density Functional Theory (TD-DFT) calculations and electro-optical absorption measurements; and the increased affinity of MC to metal ions capable of forming coordination complexes [15]. Spiropyrans have a unique feature: responsiveness to various stimuli that leads to the mentioned isomerization, such as responses to temperature (thermochromism)[16], solvent polarity (solvatochromism) [17], pH [18,19], mechanical force [20], and redox potential [21].

Spiropyrans with organic groups such as nitro, carboxyl, or hydroxyl, exhibit a phenomenon called negative photochromism in most solvents, due to the stability achieved by the zwitterionic MC form [22]. This behavior also occurs in high-polarity media, in the formation of metal complexes with MC, and when MC is embedded in a polymeric matrix [23]. Intermolecular interactions between solvent and solute are one of the main reasons that can explain the stability of the MC in certain solvents since these interactions are responsible for modifying the ground and excited state of the molecules, leading to changes in its UV—vis absorption bands [17].

Many studies of potential applications of spiropyrans have been done, such as molecular switches (on/off systems)[24], sensor for ions [25], drug release systems [26], photo-controlled enzymatic activity, photocontrol of nanoparticle solubility [27], and other studies reporting its use in coordination complexes [28]. In this sense, studies involving spiropyrans are growing, and the way that spiropyrans and metal ions interact still need to be elucidated, including some characteristics of how the molecule and the metal interact, such as binding site, molecular geometry, and chemical stability. Recently, our research group demonstrated the capabilities of SPCOOH to coordinate with Co^{2+} in its MC form [29]. Herein we have combined experimental and theoretical approaches to understand and demonstrate how zinc (II) is coordinated to SPCOOH, utilizing the UV-induced precipitation method of our previous work. We have also investigated the photo resistance, solvatochromic and photochromic properties, and the electronic structure of the complex. With the results obtained in this work, we expect to contribute with the promising field of photodynamics, represented, for instance, by a recent publication describing spiropyran systems for acetylsalicylic acid drug delivery [30].

2. Experimental section

2.1. Reagents

All reagents from the following suppliers were used without purification: 2,3,3-Trimethylindolenine (98%), 3-Iodopropanoic acid (95%), 2-Hydroxy-5-nitrobenzaldehyde (98%), 4-Methylpiperidine (96%), Tetrahydrofuran (THF) anhydrous (≥99.9%), Diethyl ether (Et_2O) anhydrous (≥99.0%), Acetonitrile (MeCN) anhydrous (99.8%), Methanol (MeOH) (≥99.8%), and 2-Butanone (MEK, ≥ 99.0%) from Sigma-Aldrich; N,N-Dimethylformamide (DMF), from Êxodo Científica (>99.8%); Ethanol (EtOH, 99.5%) and Isopropanol (>99.5%), from Quimex; Dimethyl sulfoxide (DMSO, 99.5%), from Nuclear; Acetone (Ace, 99.5%), from Anidrol; and Zinc (II) nitrate hexahydrate ($Zn(NO_3)_2{\cdot}6H_2O$, 98%), from Sigma-Aldrich.

2.2. Ligand and coordination complex synthesis

Spiropyran (SPCOOH), (1-(β-Carboxyethyl)-3′,3′-dimethyl-6-nitrospiro (indoline-2′,2 [2*H*-1] benzopyran), was synthesized according to the literature [31], with a single modification consisting of using 4-methylpiperidine instead of piperidine. ZnMC was prepared using anhydrous THF by adding $Zn(NO_3)_2{\cdot}6H_2O$ (1.35×10^{-4} mol) to SPCOOH (2.70×10^{-4} mol), under N_2 atmosphere. The THF solution of SPCOOH was previously exposed to UV radiation (at 365 nm), giving rise to a purple solution before adding the Zn^{2+} THF solution. After the addition of the metal ion solution into the SPCOOH solution, a color change can be observed, from purple to reddish-orange. This solution was kept under stirring for 1 h at room temperature and then added to cold anhydrous Et_2O, in a ratio of 5:1 Et_2O:reaction solution, and later irradiated with UV light (365 nm), leading to the precipitation of a red powder. This process was done according to the literature [29].

2.3. Experimental characterization

FTIR-ATR spectra of SPCOOH and ZnMC were recorded using a PerkinElmer Spectrum 100 instrument equipped with a diamond crystal ATR module (wavelength range of 650—4000 cm^{-1}, 4 cm^{-1}

resolution, and 64 scans). All UV−visible absorption spectra were obtained at 20 ± 1 °C. Spectra were measured in the UV−visible range (from 200 to 800 nm) using a Varian Cary 50 Scan spectrophotometer and quartz cuvettes with a path length of 10 mm and 1.5 mL. UV−visible spectra using MeOH, IPA, EtOH, MeCN, DMSO, DMF, Ace, MEK, and THF were obtained, in order to characterize the ZnMC solvatochromism. The kinetics experiment was carried out during a 16-h period for THF and a 48-h period for MeCN, obtaining an absorption spectrum every 1 min for the first hour and every 5 min for the remaining time, with a scan rate of 2400 nm per minute.

The synthesized complex was resuspended in methanol. Samples were submitted to mass spectrometry analysis in an Autoflex III Smartbeam MALDI TOF/TOF spectrometer (Bruker Daltonics, Billerica, USA). The sample was diluted in 1:1 ratio with α-cyano-4-hydroxycinnamic acid matrix (Sigma-Aldrich, Saint Louis, USA) and spotted in an MTP 384 Polished Steel target plate (Bruker Daltonics, Billerica, USA). Sample-matrix co-crystallization was carried out by the dried-droplet method [32]. External calibration was performed by homogenizing the Peptide Calibration Standard II (Bruker Daltonics, Billerica, USA) in 1:1 ratio in α-Cyano-4-hydroxycinnamic acid matrix directly on the same target plate. MS spectrum was obtained in positive reflected mode with 300 laser shots and an acceleration voltage held at 15−20 kV.

NMR spectroscopy studies were performed in a Bruker AVANCE 400 MHz spectrometer with acetonitrile-d3 as the solvent. Emission spectra were obtained in a Cary Eclipse fluorescence spectrophotometer with quartz cuvettes of 10 mm path length.

2.4. Computational details

Density Functional Theory (DFT) calculations for ZnMC (**1**), ZnMC (**2**) and MC were carried out using the Gaussian 09 (revision D.01) software package [33]. The geometries were optimized using the B3LYP[34] [−] [36] functional and the 6-31G(d) [37] basis set for all the atoms. Other works support this combination of functional and basis set for calculations of spiropyrans compounds [38−40] since larger basis sets present little influence on the accuracy [41−44] or either molecular and geometrical parameters. Solvation was taken into account by using an implicit solvation model through the Integral Equation Formalism Polarizable Continuum Model (IEFPCM)[45] for MeCN, $\varepsilon = 35.688$. Vibrational analyses, in the same theory level, were performed to ensure that the geometries are true energy minima, to verify the thermodynamic parameters, and to obtain infrared spectra. The theoretical UV−vis absorption spectra were calculated with Time-Dependent Density Functional Theory (TD-DFT) methods using the 40 lowest singlet excited states of the complex MeCN solutions. Charges from electrostatic potential using a grid-based method [46] (CHelpG) calculations were made in order to define the charge distribution for the atoms, and the Van der Waals radius used for the Zinc atom was 139 p.m [47]. The ^{1}H NMR shielding tensors for the ZnMC (1) were calculated using the GIAO (Gauge-Independent Atomic Orbital) method [48], using the same level of theory of the geometry optimizations, including the implicit solvation effect of the MeCN through IEFPCM.

3. Results and discussion

3.1. Fourier transform infrared spectroscopy with attenuated total reflectance (FTIR-ATR)

Solid complexes were obtained through a precipitation process induced by UV irradiation (Figure SI-1 − Supplementary Information) and used for all analyses reported in this work. The FTIR-ATR spectra of both the free ligand (SPCOOH) and the zinc complex (ZnMC) are presented in Fig. 2 with some important regions highlighted, which are crucial in determining the coordination sites that may be involved in the complex formation. Some bands in the spectra of the ligand are expected to change, position-wise, upon coordinating to the metal center. In the comparison between spectra, it is found that the carbonyl stretching (νC = O) of the carboxylic acid presents itself at 1708 cm^{-1} for the free ligand and this band is shifted to lower wavenumbers in the complex, at 1591 cm^{-1}, which is the first indicator that the carbonyl oxygen in the carboxylic acid participated in the coordination process [29]. The SPCOOH FTIR-ATR spectrum also shows two bands at 1270 and 1028 cm^{-1}, which are respectively attributed to the antisymmetric and symmetric stretching of the aromatic ether (C−O−C) that is substituted by a phenolate stretching band in the ZnMC spectrum at 1289 cm^{-1} [24]. These changes in the ZnMC spectrum are indications that the Zn^{2+} coordinated through the carbonyl and phenolate moieties of the MC isomer, as similarly reported in other articles [49,50].

3.2. Mass spectrometry (MALD-TOF)

MALDI TOF/TOF mass spectrometry was also utilized to characterize ZnMC. It can be observed from the MS spectrum (Figure SI-2 − Supporting Information) that the solid complex is formed by two MC molecules and a nitrate coordinated to the zinc center, with $m/z = 885.0$ for the $[M]^+$. Each ligand coordinates through two sites, forming an octahedral complex (ZnMC (**2**)), which will be discussed further in the theoretical calculations section. A peak at 823.1 m/z can also be found, which refers to the complex without the nitrate coordinated and with a coordination to two MC

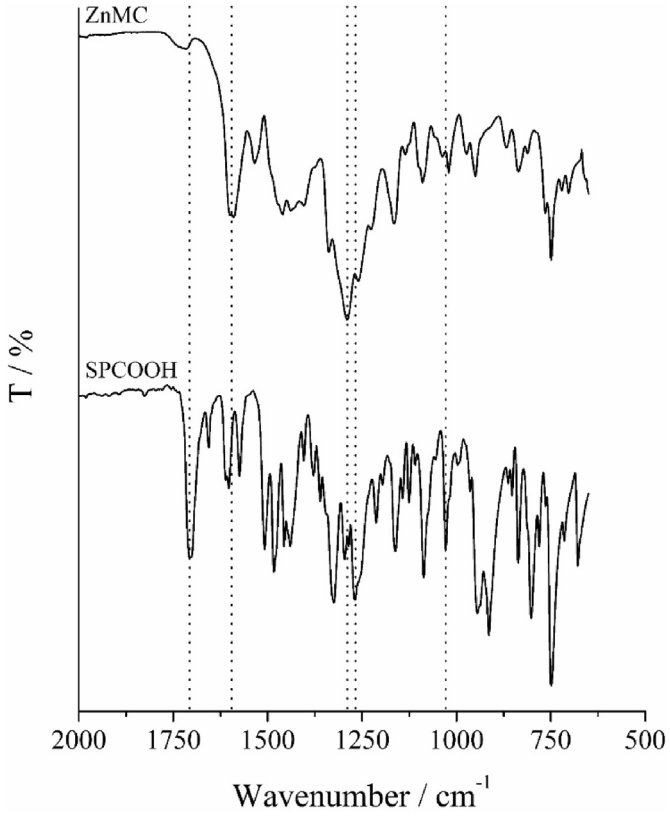

Fig. 2. FTIR-ATR spectra of the ZnMC complex (top) and the free ligand SPCOOH (bottom).

molecules arranged in a distorted tetrahedral geometry (ZnMC (**1**)). The tetrahedral complex presents a high abundance relative to the hexacoordinated one.

3.3. Nuclear magnetic resonance (NMR)

SPCOOH and ZnMC were also analyzed by means of ^{1}H NMR spectroscopy (Figure SI-3 and chemical shifts (δ) for hydrogen in Tables SI–3) in solutions of acetonitrile-$_{d3}$, and the spectra of ^{1}H can be seen in Figure SI-3b. For ZnMC, signals equivalent to the free ligand can be found (Figure SI-3a), which will be approached below. Besides, homonuclear correlations ^{1}H/^{1}H were used to assign ZnMC's hydrogens (Figure SI-3c and SI-3d). The signal observed in 1.75 for ZnMC was attributed to the methyl hydrogens, which were utilized as a reference for the integration of the other signals and fixed as equivalent to six hydrogens. Both signals in the region between 3.7 and 3.4 can be attributed to the two groups of methylene hydrogens of SPCOOH in its free form. However, ZnMC's methylene hydrogens can be assigned to the broad signal at 2.9 and the second signal in 4.6; the latter could be integrated with a value of two. The signals relating to the aromatic hydrogen's region of the spiropyran molecule coordinated are seen in the region between 6.5 and 8.6; the sum of their integrations is compatible with the expected number.

The remaining signals present in this same region can be assigned to the free ligand SPCOOH. This result can be confirmed by the chemical shift compatible with those observed in Figure SI-3b; moreover, the signals close to 8 may be covered by the ZnMC signal. The signal at 5.9 was also integrated from the ZnMC spectrum, which is relative to one hydrogen (H-14) of the ligand, resulting in an approximate value of 0.1. When comparing its integration with that of signals equivalent to one hydrogen, it can be inferred that the proportion of SPCOOH in the ZnMC sample is approximately 10%. The presence of the ligand may be correlated with the equilibrium between the coordinate and the free forms that can coexist in a solution equilibrium, even when maintained in the absence of radiation.

3.4. UV–Vis absorption spectroscopy

Among the information UV–vis absorption spectroscopy can provide, the occurrence of binding events is one of its most useful. Spiropyrans, as previously mentioned, can be found in its colorless closed-ring form, labeled SP, and its colored open-ring form, named MC. When in SP form, they are known to display two absorption bands in the UV region of the spectrum, which are attributed to π-π* electronic transitions between the two halves of the molecule, in the regions of indoline and benzospyran [51]. After exposure to UV radiation (λ = 365 nm), the isomerization gives rise to the MC form, which presents a broad band at 563 nm in MeCN (Figure SI-4), for SPCOOH. This band in the visible region of the spectrum detected for MC refers to the extensive π-electron conjugation present in the molecule after the ring-opening isomerization. A comparison between ZnMC (curve I, Fig. 3) and MC's absorption spectra obtained in solution of MeCN reveals a blue shift of 73 nm for the bands in the visible region of the spectrum, with the maximum absorbance for MC at 563 nm and 490 nm for the ZnMC complex; this is another indicator of the occurrence of the complexation reaction.

In Fig. 3, the emission spectra for ZnMC in two different excitation wavelengths (curves II and III, Fig. 3) can be observed, and it was found that the intensity of the fluorescence is higher at 490 nm. The MC isomer of spiropyrans is also known to present fluorescent properties, for the same reason mentioned above. However, at similar molar concentrations in comparison with the complex, the MC fluorescence was not observed (curve IV, Fig. 3), meaning that

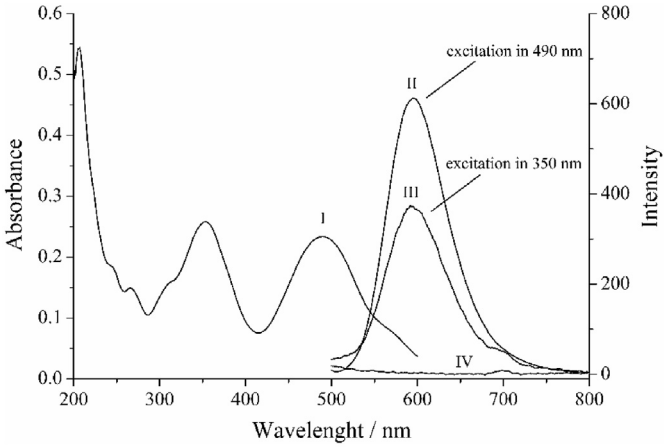

Fig. 3. UV–vis absorption spectra of ZnMC (2.1×10^{-5} mol/L) (I) in acetonitrile. Fluorescence emission spectra of ZnMC (2.5×10^{-5} mol/L) at the excitation wavelengths of 490 nm (II) and 350 nm (III), and SPCOOH (5.5×10^{-5} mol/L) (IV) in MeCN.

its fluorescence was highly intensified after forming a complex with the zinc ion. This increase in the fluorescence intensity may be attributed to the complex mainly due to zinc, as it has been shown in other reports that not every spiropyran complex exhibits this behavior [28]. The emission spectra were obtained by scanning the maximum excitation wavelength and fixing those wavelengths for the complex, using MeCN as the solvent. It is worth noting that SPCOOH was previously exposed to 5 min of UV radiation before the spectrum was obtained.

A kinetics experiment of the complex dissociation was performed (Figure SI-5) to evaluate ZnMC stability in solution, which is also a property of interest when dealing with spiropyrans. ZnMC solutions using tetrahydrofuran (THF) and acetonitrile (MeCN) were compared. Using THF, a sharp decline in the absorbance was observed in the first hour of analysis, followed by stabilization at, approximately, 400 min; the total time of analysis was 16 h (960 min). In MeCN, however, the absorbance presented a minor decline (of about 5%) in the first hour and then remained stable throughout the rest of the analysis, which lasted for a total of 48 h (2880 min), showing that ZnMC is stable in MeCN if there is no influence of radiation in the system.

3.5. Theoretical calculations

The geometrical parameters of the coordination site for both complexes, obtained through the methodology presented in section 2.4 (Fig. 4 and Tables SI–6), presents the ZnMC (**1**) complex with a tetrahedral geometry, although slightly distorted with angles between the Zn atoms and the oxygen atoms of the ligands varying from 90.6° up to 127.8° in the coordination sphere (Tables SI–6). The ZnMC (**2**) presents a distorted octahedral geometry with the sharpest angle of 58.8° located between Zn and the oxygens of coordinated nitrate ion in the equatorial position, while the oxygens from the MC ligands coordinated to zinc atom form angles of approximately 87°. In the axial position, the coordinated atoms describe an angle of 164.7° with the metal center. The results also revealed that the complex is more stable when coordinated by two oxygens of a single nitrate instead of one oxygen of each nitrate anion. Both structures are also presented in high resolution in Figure SI-7.

Comparing the bond lengths of the C=O bond for both the phenolate carbonyl group and the carboxyl acid carbonyl of the complexes with the free MC ligand (Table 1), a small increase in the

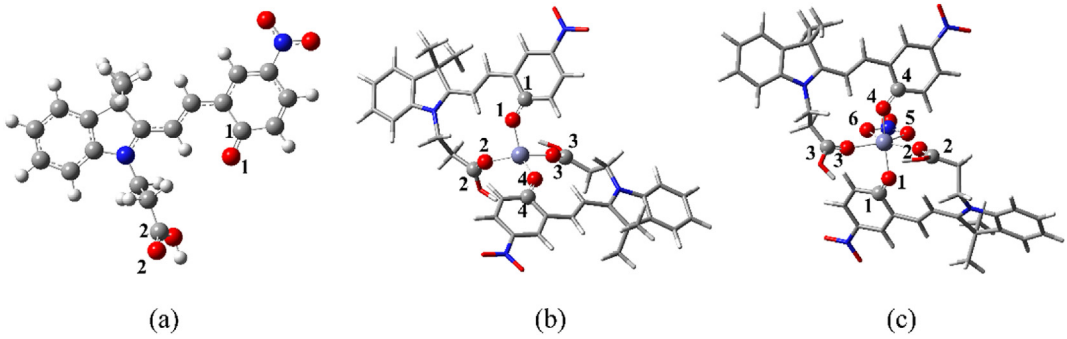

Fig. 4. Optimized structures for the (a) MC ligand, (b) ZnMC (**1**) and (c) ZnMC (**2**) complexes. Nitrate counterions were omitted in order to improve the visualization.

Table 1
Selected bond lengths (in Å) for both complexes and the free MC ligand.

Structure	C (2)–O (2)	C (3)–O (3)	C (1)–O (1)	C (4)–O (4)
MC	1.21	1.21	1.24	1.24
ZnMC (**1**)	1.24	1.25	1.29	1.29
ZnMC (**2**)	1.23	1.23	1.28	1.29

bond length for the atoms in the coordinated merocyanine was detected, meaning that the oxygens atoms are loosely bonded to the carbon due to the coordination with the zinc metal center.

The charge distribution analysis using the CHelpG methodology (Tables SI–8) confirms the coordination of the zinc atom by the oxygens of the ligands. In both zinc complex and free MC ligands, a negative charge is detected in the pyrrolic nitrogen, suggesting the absence of a zwitterionic form in the MC ligand. According to several works[38,40], such results may suggest a possible coordination site in this nitrogen, although the small ionic radius of the zinc atom and the steric hindrance from the ligands may prevent this possibility. The metallic ion presents a strong positive charge, while all coordinated oxygens have negative charges higher than those of the free MC ligand. The carbon atoms directly connected to the coordinated oxygen show an increase in the positive charge, suggesting a polarization in the bond between the atoms while coordinated. This behavior is even more pronounced in the ZnMC (2) complex.

The thermochemical parameters obtained at 298.15 K from frequency calculations revealed that the tetrahedral complex, ZnMC (**1**), is more stable in the MeCN solvent if compared with the octahedral structure, ZnMC (**2**), with a difference in the Gibbs free energy of −3.8 kcal/mol. Additionally, the change in enthalpy is −4.1 kcal/mol and the entropic term (TΔS) varies by −0.3 kcal/mol. The thermodynamics data allow concluding that, besides the tetrahedral complexes being more stable, both species exist in solution in a dynamic equilibrium situation. Therefore, an analysis of the mass spectrum leads to the conclusion that the small peak refers to the loss of the nitrate group arising from the octahedral structure, while the most dominant peaks appear due to the tetrahedral complex.

The theoretical electronic absorption spectra in the UV–vis region (Figure SI-9) in MeCN of ZnMC (**1**) presents the main band with a maximum at 455 nm (Fig. 5), while the free MC ligand presents a maximum at 497 nm in the main absorption band (experimental data $\lambda_{max} = 516$ nm). For ZnMC (**1**), the HOMO orbital is almost degenerated with the HOMO-1 orbital, showing an energy difference around 0.02 eV; the same phenomenon happens to the LUMO orbital which has an energy gap of 0.04 eV to the LUMO+1 orbital. The gaps between HOMO-1/HOMO, and LUMO/LUMO+1 in the octahedral ZnMC (2) complex, are respectively 0.05 eV and 0.04 eV, also implying some degree of degeneracy. For this reason, in Fig. 5, the presented transitions are those associated with the highest calculated oscillator strength and electronic transition participation occurring between HOMO/LUMO and HOMO-1/LUMO+1 for ZnMC **(1)**, and HOMO-1/LUMO and HOMO/LUMO+1 for ZnMC **(2)**. Both pairs of molecular orbitals, HOMO-1 and HOMO, and LUMO and LUMO+1, are almost energetically degenerated; this result is associated with small differences in the structure of the coordinated ligands in each of the complexes since they present distorted geometry.The differences in the bond lengths and dihedrals of MC ligands involved in double-bond conjugated systems contribute to the slight asymmetry of the orbitals since the molecular orbitals involved in these transitions are located at the MC ligand.

NMR calculations were carried out in order to endorse the experimental results and also to elucidate the most stable metal complex structure, ZnMC (**1**). The ^{1}H NMR δ for the selected atoms was obtained on a scale relative to TMS (tetramethylsilane) which was also optimized in the same theoretical level (Tables SI–3). The calculated δ for methyl hydrogens of ZnMC (**1**) shows good agreement with the experimental data, with a small divergence of 4% between the mean of calculated shifts (δ 1.83) and the experimental peak (δ 1.74). For the methylene hydrogens of the carboxyl acid ligand, the calculated δ are 4.47 for the H-19 (4.67 in the experimental results) and 3.49 for the H-20 (2.94 in the experimental results). The hydrogens of the indole ring (H-1, H-2, H-3, H-6) are characterized by shifts in the region from 7.35 to 7.60, while the higher shifts in the region around 7.70 and 8.83 refer to the hydrogens of benzopyran rings (H-13, H-14, H-15, H-16, H-18). Thus, the theoretical results corroborate the experimental data in which the signals of aromatic hydrogens lie in the region between 6.5 and 8.6.

The infrared spectrum was determined by vibrational analysis in the same theory level of the optimized geometry for the ZnMC (**1**) (Figure SI-10). The obtained frequency values were multiplied by a scale factor of 0.960 [52] in order to provide more accurate results. Comparisons between the experimental data (Fig. 2) and the ZnMC (**1**) theoretical spectrum are in good agreement, with the detected vibrational mode for the carbonyl stretch (νC = O) in the experimental FTIR-ATR spectrum located at 1591 cm^{-1}, while the theoretical calculations present this mode at 1622 cm^{-1}. The phenolate stretch (νC-O) for the tetrahedral complex is observed at 1300 cm^{-1}, which supports the experimental data that shows this stretching at 1289 cm^{-1} and, therefore, confirms the characterization as well as the coordination mode described in section 3.1.

3.6. Solvatochromism

Whenever changes in the chemical environment, such as

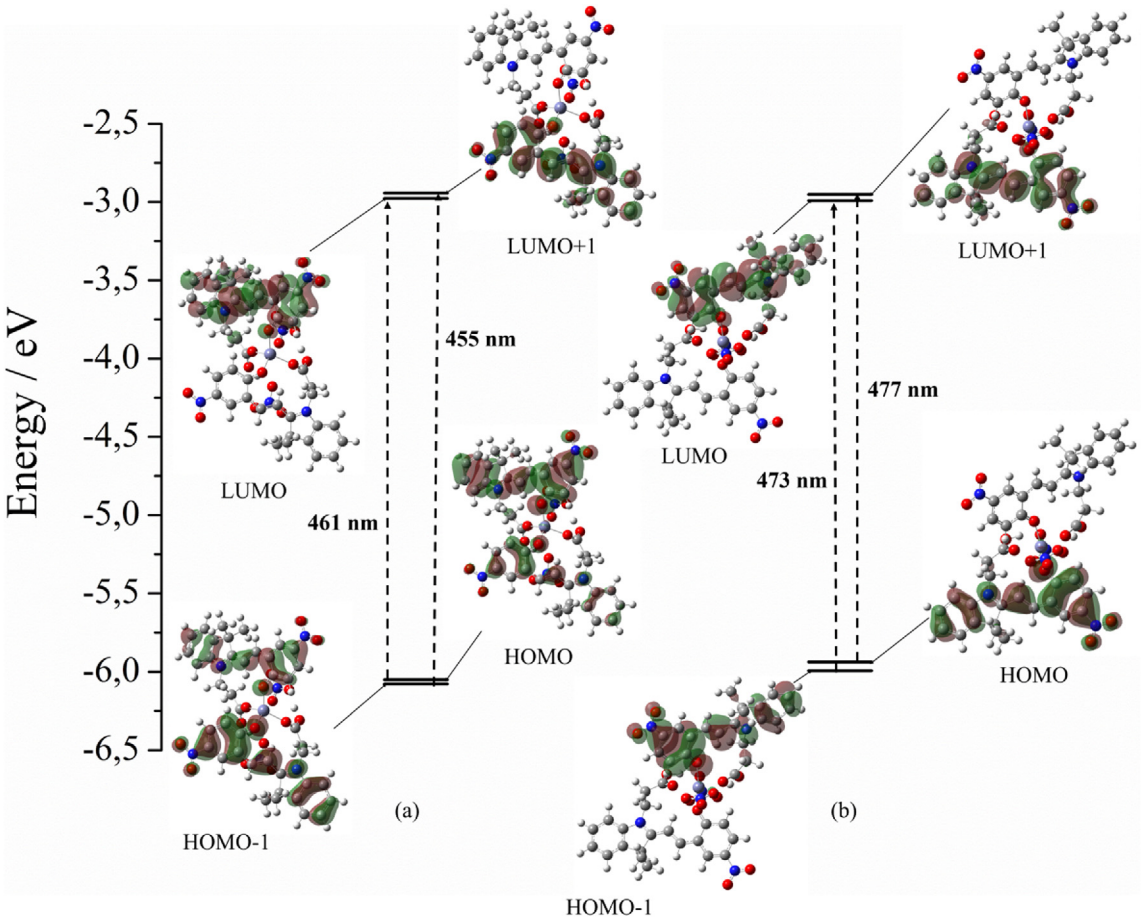

Fig. 5. Molecular orbitals participating in the main electronic transitions calculated in the UV–Vis region in MeCN for the (a) ZnMC (**1**), λ_{max} = 455 nm and (b) ZnMC (**2**), λ_{max} = 477 nm. Experimental ZnMC UV–Vis λ_{max} = 490 nm.

modifications in the polarity of solvents, cause a compound to change its color due to variations in either its absorption or emission spectra, a phenomenon that is known as solvatochromism takes place[8]. This property is usually contemplated in molecules containing an extensive π-conjugated electron system, which is the case of spiropyrans, and it is only one of the many chromisms found for this class of molecules [15]. The solvatochromic experiment was carried out in nine different solvents with distinct polarities and solvent parameters (methanol – MeOH, ethanol – EtOH, isopropanol – IPA, acetonitrile – MeCN, dimethyl sulfoxide – DMSO, dimethylformamide – DMF, acetone – Ace, 2-butanone – MEK and tetrahydrofuran – THF). The solvents were sorted in order of decreasing polarity using the Reichardt E_T (30) solvent polarity parameter [53], as presented in Table 2.

Table 2
Solvent polarity and maximum absorbance to ZnMC and MC.

Solvents	E_T (30)	λ_{ZnMC}/nm	λ_{MC}/nm [29]
MeOH	55.4	520	–
EtOH	51.9	524	538
IPA	48.4	541	–
MeCN	45.6	475	552
DMSO	45.1	563	564
DMF	43.2	563	566
Ace	42.2	486	570
MEK	41.3	414	–
THF	37.4	516	585

Results indicate that ZnMC exhibited a different absorbance maximum in each solvent (Figure SI-11), ranging from 414 to 563 nm, confirming the solvatochromic property of the complex. However, differently than what is commonly observed in free spiropyrans molecules[22],there is no clear pattern for the changes in the solvatochromic properties of ZnMC, indicating that the d orbitals of Zn^{2+} are interacting with MC's HOMOs and changing the way the intermolecular interactions affect the energy gaps between the ground and excited states in each solvent [54,55].

3.7. Reversibility experiment

The photostability of compounds containing spiropyrans is a meaningful parameter to evaluate the viability of possible applications and a property of interest reported in many recent articles [56,57]. The photostability of ZnMC was evaluated by submitting the complex to cycles of UV radiation and visible light and measuring the variation of absorbance at wavelengths of the visible region of the spectrum. The reversibility experiment was performed in MeCN and THF, with a total of 48 cycles for each solvent; each cycle consisted of 30 s of UV irradiation (λ = 365 nm) followed by 30 s of irradiation with visible light (λ = 436 nm) (Fig. 6). Results showed that ZnMC suffers from photodegradation in both solvents; although in THF (Fig. 6b) the decrease in absorbance happened slowly and constantly, in MeCN (Fig. 6a) the complex presented acceptable reversibility in the first 2 cycles and further decreases in absorbance were not observed in subsequent cycles.

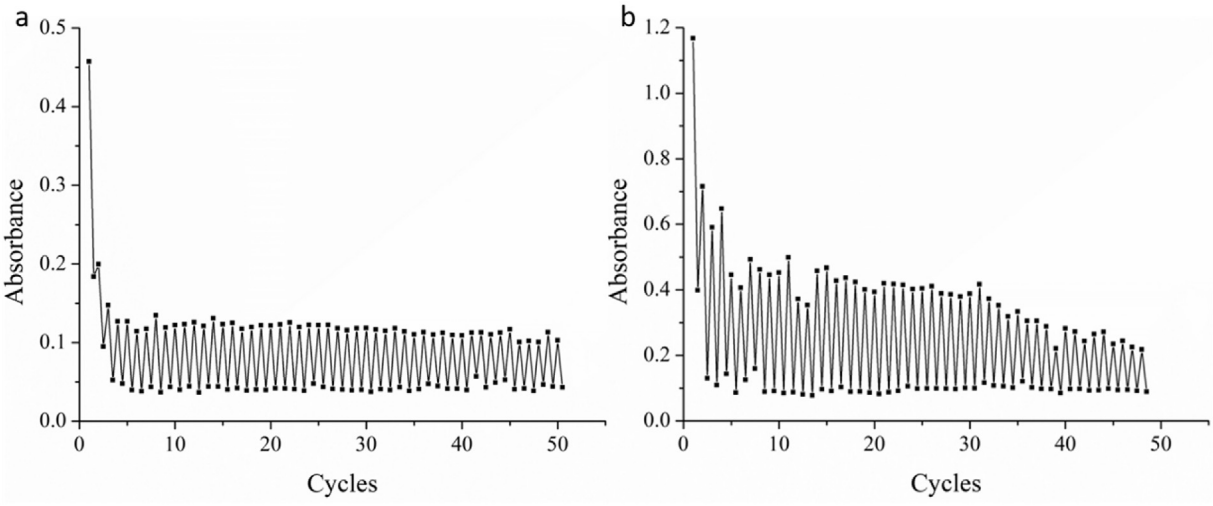

Fig. 6. Absorbance measured for switching cycles of radiation (UV and visible) for (a) MeCN at 490 nm and (b) THF at 516 nm.

4. Conclusion

We present herein a synthesized spiropyran derivative complex with zinc (II) as the metal center. Experimental characterization analyzes comprising vibrational spectroscopy, absorption spectroscopy, mass spectrometry, NMR spectroscopy, and emission spectroscopy were combined with computational methods to provide a more profound understanding of the binding aspects between SPCOOH and Zn^{2+}. Some properties of ZnMC were also studied, such as its solvatochromic characteristics, which proved not to follow any pattern regarding common solvent parameters, contrary to what is expected for spiropyrans in general. Photostability studies were also carried out for the complex in MeCN and THF, and results showed a decreasing absorbance for the complex in THF and that ZnMC is only reversible in the first 2 cycles in MeCN. This complex also has an enhanced fluorescence intensity compared to the free ligand, while retaining the characteristic reddish-orange emission of the spiropyran. These properties can be further studied for applications as sensors, fluorescent markers, and photochromic polymeric materials.

CRediT authorship contribution statement

Flávio B. Miguez: Conceptualization, Methodology, Investigation, Writing - review & editing. **Thiago G. Menzonatto:** Methodology, Investigation, Writing - original draft. **Jorge Fernandes Z. Netto:** Investigation, Writing - original draft. **Igor M.S. Silva:** Methodology, Validation, Investigation. **Thiago Verano-Braga:** Methodology, Resources, Writing - review & editing. **Juliana Fedoce Lopes:** Methodology, Resources, Writing - review & editing, Funding acquisition. **Frederico B. De Sousa:** Conceptualization, Resources, Writing - review & editing, Supervision, Project administration, Funding acquisition.

Acknowledgments

This work was supported by CAPES (scholarship 1780395 and 1828566), CNPq (grant numbers 431133/2018−2; 306726/2017−3 and scholarship 380108/2019−4) and FAPEMIG (grant numbers APQ-00403-17 and APQ-01293-14). The authors acknowledge the "Laboratório Multiusuários de Proteômica (LMProt) − Centro de Laboratórios Multiusuários (CELAM), ICB-UFMG" for technical support in the mass spectrometry analysis, and Departamento de Química − UFMG for NMR (Laboratório de Ressonância Magnética Nuclear − LAREMAR) and Emission spectra facilities, and kindly to Professor Tiago Antônio da Silva Brandão for helpful assistance.

Appendix A. Supplementary data

Supplementary data to this article can be found online at https://doi.org/10.1016/j.molstruc.2020.128105.

References

[1] S. Dasari, P. Bernard Tchounwou, Cisplatin in cancer therapy: molecular mechanisms of action, Eur. J. Pharmacol. 740 (2014) 364−378, https://doi.org/10.1016/j.ejphar.2014.07.025.
[2] C. Leung, S. Lin, H. Zhong, D. Ma, Metal complexes as potential modulators of inflammatory and autoimmune responses, Chem. Sci. 6 (2015) 871−884, https://doi.org/10.1039/C4SC03094J.
[3] D.L. Ma, H.Z. He, K.H. Leung, D.S.H. Chan, C.H. Leung, Bioactive luminescent transition-metal complexes for biomedical applications, Angew. Chem. Int. Ed. 52 (2013) 7666−7682, https://doi.org/10.1002/anie.201208414.
[4] B. Kaur, N. Kaur, S. Kumar, Colorimetric metal ion sensors − a comprehensive review of the years 2011−2016, Coord. Chem. Rev. 358 (2018) 13−69, https://doi.org/10.1016/j.ccr.2017.12.002.
[5] J. An, S.J. Geib, N.L. Rosi, Cation-triggered drug release from a porous zinc-adeninate metal-organic framework, J. Am. Chem. Soc. 131 (2009) 8376−8377, https://doi.org/10.1021/ja902972w.
[6] M.K. Barman, A. Baishya, S. Nembenna, Bulky guanidinate calcium and zinc complexes as catalysts for the intramolecular hydroamination, J. Organomet. Chem. 887 (2019) 40−47, https://doi.org/10.1016/j.jorganchem.2019.02.005.
[7] A. Senthil Murugan, N. Vidhyalakshmi, U. Ramesh, J. Annaraj, In vivo bio-imaging of sodium meta-arsenite and hydrogen phosphate in zebrafish embryos using red fluorescent zinc complex, Sensor. Actuator. B Chem. 281 (2019) 507−513, https://doi.org/10.1016/j.snb.2018.10.122.
[8] P. Bamfield, M.G. Hutchings, Chromic Phenomena: Technological Applications of Colour Chemistry, second ed., Royal Society of Chemistry, Cambridge, 2010 https://doi.org/10.1039/9781849731034.
[9] R.K. Pan, S.G. Liu, S.X. Wang, G.B. Li, W.Y. Su, Q.W. Huang, Y.M. He, Synthesis, crystal structure, luminescent property and anti-esophageal tumor activity of dinuclear zinc complex based on meso-1,2,3,4-tetra(1H-benzo[d]imidazole-2-yl)butane, Zeitschrift Fur Anorg. Und Allg. Chemie. 641 (2015) 627−630, https://doi.org/10.1002/zaac.201400447.
[10] L. Wang, Q. Li, Photochromism into nanosystems: towards lighting up the future nanoworld, Chem. Soc. Rev. 47 (2018) 1044−1097, https://doi.org/10.1039/c7cs00630f.
[11] J. Andersson, S. Li, P. Lincoln, Supporting Information Photo-Switched DNA-Binding of a Photochromic Spiropyran, Stuttg), Synthesis, 2008, pp. 1−9.
[12] N.A. Murugan, S. Chakrabarti, H. Ågren, Solvent dependence of structure, charge distribution, and absorption spectrum in the photochromic merocyanine-spiropyran pair, J. Phys. Chem. B 115 (2011) 4025−4032, https://doi.org/10.1021/jp2004612.
[13] R.J. Byrne, S.E. Stitzel, D. Diamond, Photo-regenerable surface with potential for optical sensing, J. Mater. Chem. 16 (2006) 1332−1337, https://doi.org/10.1039/b516400a.

[14] S. Scarmagnani, Z. Walsh, C. Slater, N. Alhashimy, B. Paull, M. MacKa, D. Diamond, Polystyrene bead-based system for optical sensing using spiropyran photoswitches, J. Mater. Chem. 18 (2008) 5063–5071, https://doi.org/10.1039/b810080b.

[15] R. Klajn, Spiropyran-based dynamic materials, Chem. Soc. Rev. 43 (2014) 148–184, https://doi.org/10.1039/c3cs60181a.

[16] A. Julià-López, J. Hernando, D. Ruiz-Molina, P. González-Monje, J. Sedó, C. Roscini, Temperature-controlled switchable photochromism in solid materials, Angew. Chem. Int. Ed. 55 (2016) 15044–15048, https://doi.org/10.1002/anie.201608408.

[17] C. Reichardt, T. Welton, Solvents and Solvent Effects in Organic Chemistry, fourth ed., Wiley-VCH, Weinheim, 2010 https://doi.org/10.1002/9783527632220.

[18] F.M. Raymo, S. Giordani, A.J.P. White, D.J. Williams, Digital processing with a three-state molecular switch, J. Org. Chem. 68 (2003) 4158–4169, https://doi.org/10.1021/jo0340455.

[19] V.K. Seiler, K. Callebaut, K. Robeyns, N. Tumanov, J. Wouters, B. Champagne, T. Leyssens, Acidochromic spiropyran-merocyanine stabilisation in the solid state, CrystEngComm 20 (2018) 3318–3327, https://doi.org/10.1039/c8ce00291f.

[20] S. Mo, Q. Meng, S. Wan, Z. Su, H. Yan, B.Z. Tang, M. Yin, Tunable mechanoresponsive self-assembly of an amide-linked dyad with dual sensitivity of photochromism and mechanochromism, Adv. Funct. Mater. 27 (2017) 1–9, https://doi.org/10.1002/adfm.201701210.

[21] K. Wagner, R. Byrne, M. Zanoni, S. Gambhir, L. Dennany, R. Breukers, M. Higgins, P. Wagner, D. Diamond, G.G. Wallace, D.L. Officer, A multiswitchable poly(terthiophene) bearing a spiropyran functionality: understanding photo- and electrochemical control, J. Am. Chem. Soc. 133 (2011) 5453–5462, https://doi.org/10.1021/ja1114634.

[22] W. Tian, J. Tian, An insight into the solvent effect on photo-, solvato-chromism of spiropyran through the perspective of intermolecular interactions, Dyes Pigments 105 (2014) 66–74, https://doi.org/10.1016/j.dyepig.2014.01.020.

[23] V.A. Barachevsky, Negative photochromism in organic systems, Rev. J. Chem. 7 (2017) 334–371, https://doi.org/10.1134/s2079978017030013.

[24] F.B. De Sousa, J.D.T. Guerreiro, M. Ma, D.G. Anderson, C.L. Drum, R.D. Sinisterra, R. Langer, Photo-response behavior of electrospun nanofibers based on spiropyran-cyclodextrin modified polymer, J. Mater. Chem. 20 (2010) 9910–9917, https://doi.org/10.1039/c0jm01903h.

[25] R.C.L. Machado, F. Alexis, F.B. De Sousa, Nanostructured and photochromic material for environmental detection of metal ions, Molecules 24 (2019) 4243, https://doi.org/10.3390/molecules24234243.

[26] R. Tong, H.D. Hemmati, R. Langer, D.S. Kohane, Photoswitchable nanoparticles for triggered tissue penetration and drug delivery, J. Am. Chem. Soc. 134 (2012) 8848–8855, https://doi.org/10.1021/ja211888a.

[27] E.I. Balmond, B.K. Tautges, A.L. Faulkner, V.W. Or, B.M. Hodur, J.T. Shaw, A.Y. Louie, Comparative evaluation of substituent effect on the photochromic properties of spiropyrans and spirooxazines, J. Org. Chem. 81 (2016) 8744–8758, https://doi.org/10.1021/acs.joc.6b01193.

[28] M. Baldrighi, G. Locatelli, J. Desper, C.B. Aakeröy, S. Giordani, Probing metal ion complexation of ligands with multiple metal binding sites: the case of spiropyrans, Chem. Eur J. 22 (2016) 13976–13984, https://doi.org/10.1002/chem.201602608.

[29] F.B. Miguez, I.F. Reis, L.P. Dutra, I.M.S. Silva, T. Verano-Braga, J.F. Lopes, F.B. De Sousa, Electronic investigation of light-induced reversible coordination of Co(II)/spiropyran complex, Dyes Pigments (2019) 107757, https://doi.org/10.1016/j.dyepig.2019.107757.

[30] F. Cardano, E. Del Canto, S. Giordani, Spiropyrans for light-controlled drug delivery, Dalton Trans. (2019), https://doi.org/10.1039/C9DT02092F.

[31] A. Fissi, O. Pieroni, G. Ruggeri, F. Ciardelli, Photoresponsive polymers. Photomodulation of the macromolecular structure in poly(L-lysine) containing spiropyran units, Macromolecules 28 (1995) 302–309, https://doi.org/10.1021/ma00105a042.

[32] R.C. Beavis, T. Chaudhary, B.T. Chait, α-Cyano-4hydroxycinnamic acid as a matrix for matrix- assisted laser desorption mass-spectrometry, Org. Mass Spectrom. 27 (1992) 156–158, https://doi.org/10.1002/oms.1210270217.

[33] M.J. Frisch, G.W. Trucks, H.B. Schlegel, G.E. Scuseria, M.A. Robb, J.R. Cheeseman, G. Scalmani, V. Barone, B. Mennucci, G.A. Petersson, H. Nakatsuji, M. Caricato, X. Li, H.P. Hratchian, A.F. Izmaylov, J. Bloino, G. Zheng, J.L. Sonnenberg, M. Hada, M. Ehara, K. Toyota, R. Fukuda, J. Hasegawa, M. Ishida, T. Nakajima, Y. Honda, O. Kitao, H. Nakai, T. Vreven, J.A.J. Montgomery, J.E. Peralta, F. Ogliaro, M. Bearpark, J.J. Heyd, E. Brothers, K.N. Kudin, V.N. Staroverov, T. Keith, R. Kobayashi, J. Normand, K. Raghavachari, A. Rendell, J.C. Burant, S.S. Iyengar, J. Tomasi, M. Cossi, N. Rega, J.M. Millam, M. Klene, J.E. Knox, J.B. Cross, V. Bakken, C. Adamo, J. Jaramillo, R. Gomperts, R.E. Stratmann, O. Yazyev, A.J. Austin, R. Cammi, C. Pomelli, J.W. Ochterski, R.L. Martin, K. Morokuma, V.G. Zakrzewski, G.A. Voth, P. Salvador, J.J. Dannenberg, S. Dapprich, A.D. Daniels, O. Farkas, J.B. Foresman, J.V. Ortiz, J. Cioslowski, D.J. Fox, Gaussian 09, Revision D.01, Gaussian Inc., Wallingford CT, 2013.

[34] A.D. Becke, Density-functional thermochemistry. III. The role of exact exchange, J. Chem. Phys. 98 (1993) 5648–5652, https://doi.org/10.1063/1.464913.

[35] C. Lee, C. Hill, N. Carolina, Development of the Colle-Salvetti correlation-energy formula into a functional of the electron density, Chem. Phys. Lett. 162 (1988) 165–169, https://doi.org/10.1016/0009-2614(89)85118-8.

[36] A.D. Becke, Density-functional exchange-energy approximation with correct asymptotic behavior, Phys. Rev. 38 (1988) 3098–3100, https://doi.org/10.1103/PhysRevA.38.3098.

[37] W.J. Hehre, K. Ditchfield, J.A. Pople, Self-consistent molecular orbital methods. XII. Further extensions of Gaussian-type basis sets for use in molecular orbital studies of organic molecules, J. Chem. Phys. 56 (1972) 2257–2261, https://doi.org/10.1063/1.1677527.

[38] G. Cottone, R. Noto, G. La Manna, Theoretical study of spiropyran-merocyanine thermal isomerization, Chem. Phys. Lett. 388 (2004) 218–222, https://doi.org/10.1016/j.cplett.2004.03.016.

[39] Y. Sheng, J. Leszczynski, A.A. Garcia, R. Rosario, D. Gust, J. Springer, Comprehensive theoretical study of the conversion reactions of spiropyrans: substituent and solvent effects, J. Phys. Chem. B 108 (2004) 16233–16243, https://doi.org/10.1021/jp0488867.

[40] G. Balasubramanian, J. Schulte, F. Müller-Plathe, M.C. Böhm, Structural and thermochemical properties of a photoresponsive spiropyran and merocyanine pair: basis set and solvent dependence in density functional predictions, Chem. Phys. Lett. 554 (2012) 60–66, https://doi.org/10.1016/j.cplett.2012.10.014.

[41] P.C. Hariharan, J.A. Pople, The effect of d-functions on molecular orbital energies for hydrocarbons, Chem. Phys. Lett. 16 (1972) 217–219, https://doi.org/10.1016/0009-2614(72)80259-8.

[42] A. Broo, A. Holmén, Ab initio MP2 and DFT calculations of geometry and solution tautomerism of purine and some purine derivatives, Chem. Phys. 211 (1996) 147–161, https://doi.org/10.1016/0301-0104(96)00184-X.

[43] A. Holmén, A. Broo, A theoretical investigation of the solution N(7) H⇆N(9) H tautomerism of adenine, Int. J. Quant. Chem. 56 (1995) 113–122, https://doi.org/10.1002/qua.560560712.

[44] W.J. Hehre, L. Radom, P.v.R. Schleyer, J.A. Pople, Ab Initio Molecular Orbital Theory, first ed., Wiley-Interscience, New York, 1986.

[45] E. Cancès, B. Mennucci, J. Tomasi, A new integral equation formalism for the polarizable continuum model: theoretical background and applications to Isotropic and anisotropic dielectrics, J. Chem. Phys. 107 (1997) 3032–3041, https://doi.org/10.1063/1.474659.

[46] C.M. Breneman, K.B. Wiberg, Determining atom-centered monopoles from molecular electrostatic potentials. The need for high sampling density in formamide conformational analysis, J. Comput. Chem. 11 (1990) 361–373, https://doi.org/10.1002/jcc.540110311.

[47] A. Bondi, Van der waals volumes and radii, J. Phys. Chem. 68 (1964) 441–451, https://doi.org/10.1021/j100785a001.

[48] K. Wolinski, J.F. Hinton, P. Pulay, Efficient implementation of the gauge-independent atomic orbital method for NMR chemical shift calculations, J. Am. Chem. Soc. 112 (1990) 8251–8260, https://doi.org/10.1021/ja00179a005.

[49] K.H. Fries, J.D. Driskell, S. Samanta, J. Locklin, Spectroscopic analysis of metal ion binding in spiropyran containing copolymer thin films, Anal. Chem. 82 (2010) 3306–3314, https://doi.org/10.1021/ac1001004.

[50] Y. Xue, P. Gong, J. Tian, Specific recognition of Cu2+by simple spiropyran via forming a ternary complex of spiropyran-Cu2+-DMF, Colloids Surfaces A Physicochem. Eng. Asp. 541 (2018) 165–174, https://doi.org/10.1016/j.colsurfa.2018.01.017.

[51] N.W. Tyer, R.S. Becker, Photochromic spiropyrans. I. Absorption spectra and evaluation of the π-electron orthogonality of the constituent halves, J. Am. Chem. Soc. 92 (1970) 1289–1294, https://doi.org/10.1021/ja00708a031.

[52] K.K. Irikura, R.D. Johnson, R.N. Kacker, Uncertainties in scaling factors for ab initio vibrational frequencies, J. Phys. Chem. 109 (2005) 8430–8437, https://doi.org/10.1021/jp052793n.

[53] C. Reichardt, Solvatochromic dyes as solvent polarity indicators, Chem. Rev. 94 (1994) 2319–2358, https://doi.org/10.1021/cr00032a005.

[54] F.A. Cotton, G. Wilkinson, C.A. Murillo, M. Bochmann, Advanced Inorganic Chemistry, sixth ed., Wiley, New York, 1999.

[55] C. Reichardt, T. Welton, Solvents and Solvent Effects in Organic Chemistry, fourth ed., Wiley-VCH, Weinheim, Germany, 2010.

[56] G.M. Sylvia, S. Heng, A. Bachhuka, H. Ebendorff-Heidepriem, A.D. Abell, A spiropyran with enhanced fluorescence: a bright, photostable and red-emitting calcium sensor, Tetrahedron 74 (2018) 1240–1244, https://doi.org/10.1016/j.tet.2017.11.020.

[57] M.H. Sharifian, A.R. Mahdavian, H. Salehi-Mobarakeh, Effects of chain parameters on kinetics of photochromism in acrylic-spiropyran copolymer nanoparticles and their reversible optical data storage, Langmuir 33 (2017) 8023–8031, https://doi.org/10.1021/acs.langmuir.7b01869.